



**Quantum transport in oxidized Ni nanocontacts under mechanical strain**Zahra Razavifar <sup>1,2</sup>, Alireza Saffarzadeh <sup>1,3,\*</sup> and J. J. Palacios<sup>2</sup><sup>1</sup>*Department of Physics, Payame Noor University, P.O. Box 19395-3697 Tehran, Iran*<sup>2</sup>*Departamento de Física de la Materia Condensada, Instituto Nicolás Cabrera (INC), and Condensed Matter Physics Center (IFIMAC), Universidad Autónoma de Madrid, 28049 Madrid, Spain*<sup>3</sup>*Department of Physics, Simon Fraser University, Burnaby, British Columbia, Canada V5A 1S6*

(Received 26 March 2020; accepted 9 June 2020; published 25 June 2020)

We report density functional theory based simulations of the final stages in the formation process of oxidized Ni nanocontacts along with their measurable conductance under mechanical strain. Not surprisingly, the presence of O atoms drastically changes the overall conductance as well as its spin polarization character. We have considered up to two O atoms in our simulations and found that their placement near the atomic constriction largely determines the conductance values. An overall picture emerges where the stability of the nanocontact improves with respect to that of pure Ni ones, supporting longer elongations as seen in the experiments. Also a remarkable effect takes place: the emergence of half metallicity (a fully spin polarized current), which seems to be a robust effect, but not necessarily translated into a very large magnetoresistance.

DOI: [10.1103/PhysRevB.101.235442](https://doi.org/10.1103/PhysRevB.101.235442)**I. INTRODUCTION**

Electronic transport through atomic contacts, atomic chains, or molecular junctions, where molecules are suspended between two metallic electrodes, has been widely investigated both experimentally and theoretically for more than a decade. These studies are relevant because of the understanding we gain towards the fabrication, performance, and possible applications of nanoelectronic devices [1]. In this regard progress has been slow since many variables enter the picture, all of them playing key roles in determining the conductance and current flow: contact geometries, electronic hybridization, molecule conformations and molecular electronic structure, the chemical nature of electrodes, etc. For instance, uncontrolled geometrical changes occur while varying the separation between the two metal electrodes of the nanocontact or molecular junction to name an example; recent theoretical and experimental studies have indicated that the stretching of the junctions not always results in the weakening of the interatomic bonds and a concomitant reduction of its conductance, but in some cases the mechanical pulling leads to the shift of the highest occupied molecular orbital (HOMO) toward the Fermi level of the electrodes and enhancement of the conductance [2–4].

The controlled use of the electron spin in addition to its charge increases the versatility of electronic nanodevices in terms of information processing and has led to a new branch of nanoscience known as spintronics. The origin of spintronics can be, arguably, traced back to the observation of spin-polarized electron injection from a ferromagnetic metal to normal metal [5] and the discovery of the giant magne-

toresistance (GMR) effect independently by Baibich *et al.* and Binasch *et al.* [6,7]. Since then, much effort has been made to explore and design optimal GMR devices, spin-filter transistors, advanced magnetic sensors, and random access memories with substantially improved features which usually require highly spin polarized currents (good spin filtering).

Some basic understanding has been obtained over the years studying, both theoretically and experimentally, atomic and molecular junctions based on ferromagnetic metal electrodes starting from the simplest nanocontacts [8–21]. For example, based on first principles calculations, usually density functional theory (DFT), a conductance value  $1.0G_0$  has been found for a Ni-Co/Co(111) junction, although this value of conductance is not a general behavior for similar atomic junctions such as Co-Co/Co(111), Ni-Ni/Ni(111), and Ni-Ni/Ni(001) with  $1.6G_0$ ,  $3.1G_0$ , and  $3.54G_0$ , respectively [22] (hereon  $G_0 = e^2/h$  is the spin-resolved quantum of conductance, with  $e$  being the electron charge and  $h$  Planck's constant). DFT studies of a gold chain sandwiched between two cobalt electrodes showed high spin polarization of conductance about 90% caused by strong hybridization of the  $s$  and  $d_{z^2}$  orbitals at the Co-Au interface [23]. Ability to control and adjust the magnetoresistance by changing the orientation between the metal electrodes and molecule which modifies the orbital hybridization has been investigated in Ni-benzene junctions [24,25].

Recent theoretical studies have suggested a mechanism based on symmetry arguments which leads to zero overlap between the  $s$ -like channel of the ferromagnetic electrode and the  $p$  orbitals of the junction and complete suppression of one of the spin conductance channels. An infinite GMR was thus predicted for polythiophene connected to semi-infinite Ni chains while moderate values were anticipated for realistic Ni(111) electrodes [26]. As a followup of this phenomenon, a high spin-down conductance ( $G^\downarrow \approx 0.7G_0$ ,

\* Author to whom correspondence should be addressed: asaffarz@sfu.ca

$G^\uparrow \approx 0$ ) was found by connecting a quaterthiophene molecule to Fe(110) electrodes, among various other ferromagnetic metals (Fe, Co, and Ni) with different crystallographic orientations [27].

Investigation on single molecule junctions with diatomic or triatomic molecules (e.g.,  $O_2$ ,  $H_2$ ,  $N_2$ , and  $H_2O$ ) has particularly been an active area of research in nanoelectronics because of the possibility of a comprehensive comparison between various theoretical and experimental methods [28–38]. Oxygen molecules are particularly relevant. In break junction experiments with Cu and Ag metals, only short (up to two or three atoms) single atomic chains (SACs) can be formed [37], but the strength of the chains can be increased in an oxygen atmosphere (stretched up to 10 Å) [35]. Very large values of magnetoresistance in Ni point contacts in the presence of O atoms were predicted for simple model structures, but always accompanied with insulating behavior [11,13]. Simulations also demonstrated that Fe SACs incorporated with O atoms become half metallic when they are short, but, on increasing the number of O atoms, the conductance decreases and the Fe-O SACs tend to be semiconducting (more than 4 O atoms) [34]. Interestingly, the ability to produce up to 100% spin polarized current at a NiO atomic junction formed between two Ni electrodes was recently reported using the break junction technique in cryogenic conditions (4.2 K) [39].

From a nanoscience standpoint, Ni is a ferromagnetic metal that can display, as the nanocontact is formed approaching the atomic scale, magnetoresistance [10,24,40,41], the Kondo effect [15], and unexplained values of conductance right before the contact is broken [9,17,18]. A common and extended method of studying electronic transport in atomic-sized contacts consists of collecting thousands of traces of conductance versus electrodes displacement and plotting them in a conductance histogram [42,43]. (In this context displacement generally refers to the change of the interelectrode separation.) The most common histogram recorded for Ni over the years exhibits a single broad peak at around  $3.0G_0$  [9,15,18,44]. However, Ni can also exhibit histograms with two characteristic narrower peaks at approximately  $G = 2.0G_0$  and  $G = 4.0G_0$ . In the former case, the value of the main peak is in rather good agreement with DFT calculations of the electronic transport in structures based on either small nanocontact models [10] or obtained from molecular dynamics simulations [17]. The latter set of histograms featuring two peaks has not been explained so far.

Our purpose in this work is to revisit the physics of pristine and oxidized Ni nanocontacts where, as summarized above, it is known that the presence of O atoms near the constriction can drastically change their mechanical and electronic properties. Here we go beyond molecular dynamics [17] by simulating the rupture of the nanocontacts via DFT calculations, which is also used in the evaluation of the electronic conductance. Our simulations also go a step further in the description of the rupture process by considering larger and more realistic nanocontacts [10,11] where the plasticity of Ni can be better captured. Also, up to two O atoms, as originating from  $O_2$  molecules, have been considered so that realistic configurations near the final rupture (last conductance plateau) can be obtained. We reproduce experimental findings

which have demonstrated that O atoms increase the stability and length of the last conductance plateau with respect to the pristine case. We also show that half metallicity is not only present in model nanocontacts, being more robust than previously imagined. However, we find that large GMR values do not necessarily result from this.

## II. METHODOLOGY

All the calculations have been carried out with our code ANT.G [45–47] which implements the nonequilibrium Green’s function formalism for quantum transport seamlessly interfacing the GAUSSIAN code [48]. Our new implementation presents an excellent scaling with the number of computer nodes, which allows us to address the present study within a reasonable time scale in local clusters. Following previous experience [10], the LDA functional is used throughout. This is based on the fact that  $d$  electrons at the Fermi level present a fairly itinerant and delocalized character. Nevertheless, a caveat should be mentioned when it comes to the presence of O atoms. It is known that due to the insufficient cancellation of the self-interaction in the local exchange functional the occupied  $3d$  bands are raised in energy. As a result the LDA underestimates the gap of bulk NiO [49]. Other approximations to the functional such as hybrid functionals correct the self-interaction error present in LDA by adding the exact non-local Hartree-Fock exchange [50]. DFT-based alternatives that correct the self-interaction error such as LDA+U and the  $GW$  approximation lead to similar results. All these corrections, on the other hand, do not improve the electronic structure of pure Ni, artificially increasing the bulk magnetic moments and decreasing the calculated conductance, both quantities, properly obtained in LDA. Since our nanocontacts are mostly Ni based, we have decided to use LDA, keeping in mind that we may be overestimating the conductance when O atoms are present.

## III. RESULTS AND DISCUSSION

### A. Pristine Ni nanocontacts

We start by revisiting the conductance of pure Ni nanocontacts. We assume, as the simplest possible scenarios, that a dimerlike or a monomerlike structure has already been formed in the last elongation stage before the final rupture. Starting from an equilibrium (minimum energy) configuration [see, e.g., first insets in Figs. 1(a) and 4(a)], assumed to be preceded by a plastic deformation, we rigidly separate the outermost planes of the pyramidal electrodes by increasing their relative distance  $\Delta$  in small steps. The eight innermost atoms of the junction are allowed to relax at each step. This progressive separation results in a pulling force sustained until breakup [see last inset in Fig. 1(a)], defined by the absence of interaction between the two metallic pieces and, thereby, the absence of force. For this simulation, all spins are taken to be aligned in a parallel (P) or fully ferromagnetic spin configuration.

Figure 1 shows the conductance, given by the transmission at the Fermi energy,  $E_F$ , in units of conductance quantum,  $G_0 = e^2/h$ , as a function of  $\Delta$  for the dimer case, both when all the spins are aligned in the P configuration [panel (a)]

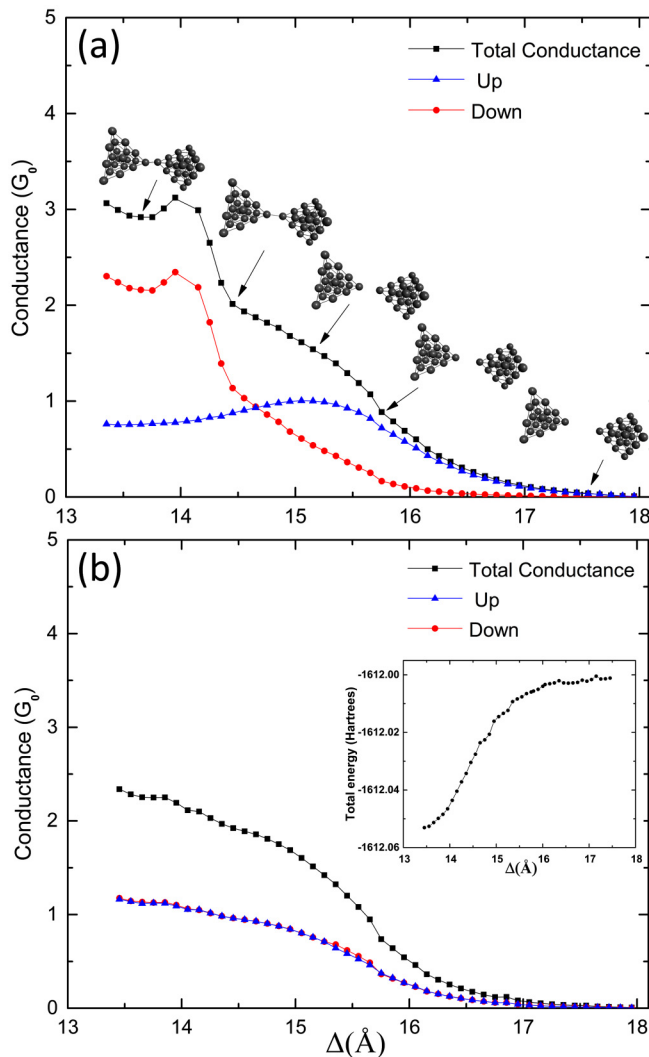


FIG. 1. Spin-resolved and total conductance at the Fermi energy as a function of  $\Delta$  for a dimer nanocontact based on an fcc Ni(111) structure in (a) parallel and (b) antiparallel magnetic configuration. Intermediate structures obtained in the elongation process are also shown in the upper panel. The inset of (b) shows total energy as a function of  $\Delta$ .

and when an abrupt domain wall is formed between the tip atoms of the respective electrodes in an antiparallel (AP) spin configuration [panel (b)]. (The same atomic structures are used for both spin configurations since the magnetic energy is typically much smaller than other contributions to the forces). For the first several steps the actual separation of the two tip atoms changes by a very small amount (up to  $\sim 0.1$  Å), manifesting good mechanical stability of the junction and resulting in a conductance plateau of  $\sim 3G_0$  [Fig. 1(a)]. This is in good agreement with a plethora of existing experimental results [15,17]. The separate contribution of the majority (up) and minority (down) spin channels shows that the plateau length depends on the behavior of the minority channel, whose contribution to the conductance is larger than that of the majority channel (because of the presence of  $d$  orbitals at  $E_F$ ), but suddenly drops below after further stretching. This can be attributed to the decay of the hopping between the tip atom

orbitals, faster for the hybridized spin-down  $sd$  orbitals than for the pure spin-up  $s$  orbitals. The spin-dependent projected density of states (PDOS) at one of the tip atoms near breakup clearly shows this [see Fig. 2(b)]. The opposite is true at the beginning of the stretching process where the PDOS of the minority  $s$  electrons dominates over that of the majority ones as shown in Fig. 2(a). Note that in order to properly simulate the last conductance plateau [the tail in the conductance at large  $\Delta$  seen in Fig. 1(a) is probably unrealistically long], more atoms should be allowed to relax to account for the actual elasticity/plasticity of Ni. Although similar DFT simulations have been reported in the past [22,51], we believe that a well-defined plateau with its concomitant conductance drop has been reproduced fully here from DFT calculations in magnetic nanocontacts.

For the AP magnetic configuration, the domain wall is located between the two Ni tip atoms of the left and right electrodes. Because of the appearance of  $s$  orbitals in a wide range of energies around  $E_F$  for both spin directions,  $s$  electrons can easily transmit between electrodes. In contrast, most of the transmission of incoming spin-down  $d$  electrons is blocked at the domain wall because these cannot find their counterpart on the receiving electrode. So, as seen in Fig. 1(b), for the AP magnetic configuration the conductance is dominated by nearly unpolarized  $s$  electrons, starting from about  $2G_0$  and decreasing smoothly without a clear trace of a plateau. At this point we can only speculate about the connection between the domain wall and the peak at  $G = 2G_0$  seen in the set of double-peak histograms. From the P and AP conductance one can obtain the MR as a function of  $\Delta$  defined as  $MR = (G_P - G_{AP})/G_{AP} \times 100$ . This is shown in Fig. 3(a). As can be seen it stays positive as a function of  $\Delta$  with sizable values before the contact is broken. Once the rupture takes place MR goes up again, but, as discussed above, this region probably extends too much in  $\Delta$  because of the excessive rigidity of the electrodes in our simulation.

We have repeated the same analysis assuming a monomer model in the last plateau before rupture [see insets in Fig. 4(a)]. Again a clear plateau with  $G \simeq 3G_0$  can be observed followed by a sudden drop in the conductance. On the basis of this result both dimer and monomer structures could, in principle, equally contribute to the main histogram peak in the one-peak histograms. The spin polarization resulting from the spin-resolved contributions to the conductance has not qualitatively changed with respect to the dimer case, presenting a sign change near the sudden conductance drop, but it has changed quantitatively. The polarization of the current in the tunneling region is larger in the dimer case. Also, a difference with respect to the dimer configuration can be noted at small displacements where the spin majority and minority contributions become similar now. This result is consistent with the PDOS shown in Figs. 2(c) and 2(d), where the spin-up  $s$  orbital contribution remains high throughout the breaking. These differences make shot-noise transport experiments more adequate to distinguish, in principle, between monomer and dimer configurations [52]. Interestingly, when a domain wall is now introduced between the single atom at the contact and the rest of atoms in one of the electrodes (this costs more magnetic energy to create in this case than in the previous dimer model), we do not observe a significant change

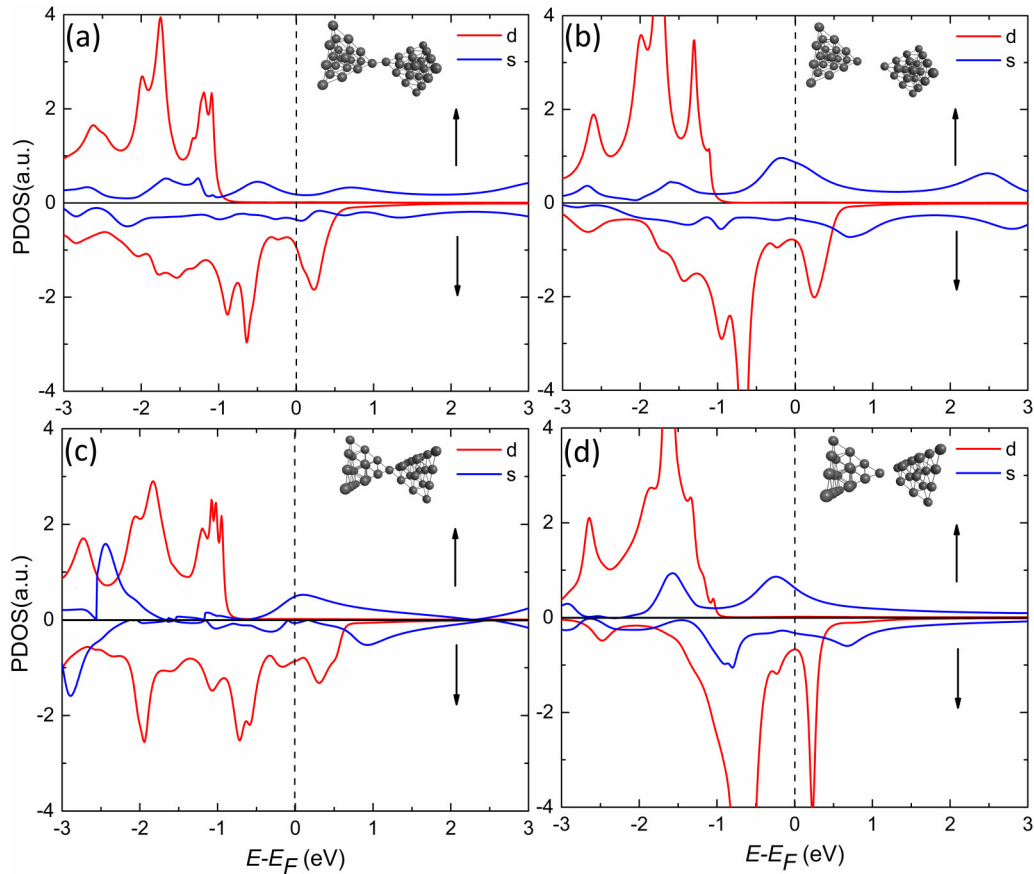


FIG. 2. Spin-polarized density of states projected on the  $s$  and  $d$  orbitals of the apex atom of one of the electrodes forming a dimer nanocontact [panels (a) and (b)] and on the single atom junction of a monomer nanocontact [panels (c) and (d)] for the structures shown in the insets. The right panels refer to the beginning of the stretching process and the left ones to near breakup of the junction.

with respect to the average P conductance and the plateau remains visible. On the other hand, MR becomes negative over most of the nanocontact evolution towards rupture. Our findings indicate that the asymmetry of the junction, actually determined by the position of the domain wall as far as the electronic structure is concerned, has a strong effect on the resulting transmission differences between spin channels.

### B. Oxidized Ni nanocontacts

Intentionally or accidentally,  $O_2$  molecules or individual O atoms may adsorb on the Ni nanocontact, the latter originating from the dissociation of  $O_2$  molecules. We thus consider a pair of O atoms in our next set of simulations. We start by adding two dissociated O atoms near the constriction, where they are more likely to affect the mechanical and electronic properties of the nanocontact. Here we restrict ourselves to dimer-type structural configurations in the P magnetic configuration. Out of the many possibilities we have chosen to start with the one shown in Fig. 5(b), where, for small electrode separations, one O atom falls between the apexes in a zigzag position, while the other sits in the vicinity. This configuration is energetically (meta)stable of minimal energy as a function of  $\Delta$  and we take it as the starting point in the simulation where  $\Delta$  is progressively increased towards total rupture as shown on Fig. 5(l). Same as for pure Ni nanocontacts, at each

incremental step of  $\Delta$ , a full relaxation is carried out giving rise to the energy evolution shown in the inset of Fig. 6(a). A few other snapshots of the whole process are shown in Fig. 5.

In the early stages of stretching the junction [up to 0.4 Å from (a) to (b) in Fig. 5], the Ni-O-Ni bond angle in the center of the structure increases by about 15°. Upon further stretching by 0.5 Å, a good mechanical (angular) stability is observed [(c) to (d) in Fig. 5]. At  $\Delta = 15.66$  Å, shown in Fig. 5(d) and labeled (d) in Fig. 6(a), the Ni-O-Ni bond angle has increased from 172° to 178° while the Ni-O bond between the Ni apex atom and the O atom located on the left electrode is broken (understood as a significant change in their relative distance). The conductance here significantly decreases to  $1.55G_0$ , defining a short plateau. By further stretching from (e) to (h), a slower reduction of the conductance occurs down to  $0.8G_0$  [see Fig. 6(a)] due to a progressive increase of the length of the Ni-Ni bond between the Ni apex atom and one of the Ni atoms of the left electrode. Interestingly, from (h) to (j), the conductance is only reduced by approximately  $0.1G_0$ , which indicates a relatively good mechanical stability at this point. From  $\Delta = 17.06$  to 20.06 Å [two intermediate structures are shown in Figs. 5(k) and 5(l)], an exponential reduction of the conductance takes place with no more bond breaking. The big picture that emerges from this simulation is that the incorporation of O atoms near the constriction helps to stabilize intermediate configurations which significantly

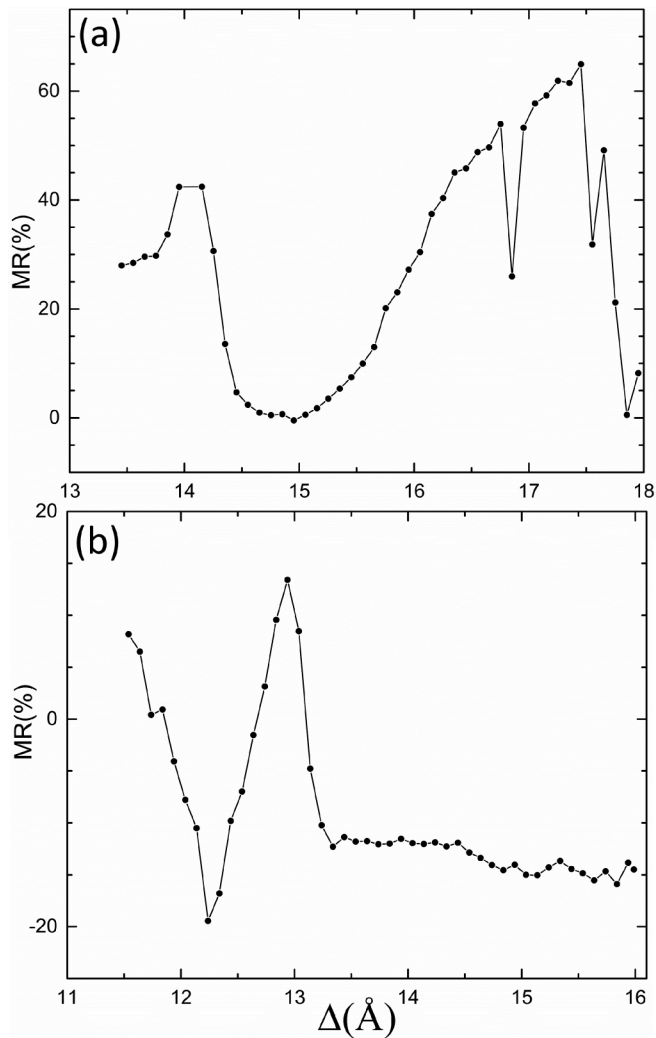


FIG. 3. Magnetoresistance as a function of electrodes distance for (a) dimer and (b) monomer nanocontacts.

increase the overall stability of the nanocontact. Note that an increased tensile strength of oxidized junctions has been experimentally reported in Ref. [39].

The spin-resolved conductance also plotted in Fig. 6(a) shows a remarkable effect: it is almost completely spin polarized, dominated by the spin minority carriers. As previous studies have shown [11,13], spin-up  $s$  electrons are not significantly present in the band structure and corresponding PDOS for an infinite one-dimensional NiO chain at the Fermi level. The hybridization of O  $p$  orbitals with the Ni  $s$  orbital leads to a shift in the  $s$  state away from  $E_F$ , resulting in almost perfect half-metallic behavior. The inset in Fig. 6(a) shows the spin-resolved transmission vs energy for the structure (g) in Fig. 5, where one can see the strong suppression of the spin-majority conductance around the Fermi energy. This result was predicted in Ref. [11] using a very ideal model of oxidized nanocontacts. Our simulations here show how robust this result is, appearing in the whole range of  $\Delta$  that goes from the formation of the last well-defined plateau all the way down to the tunneling regime.

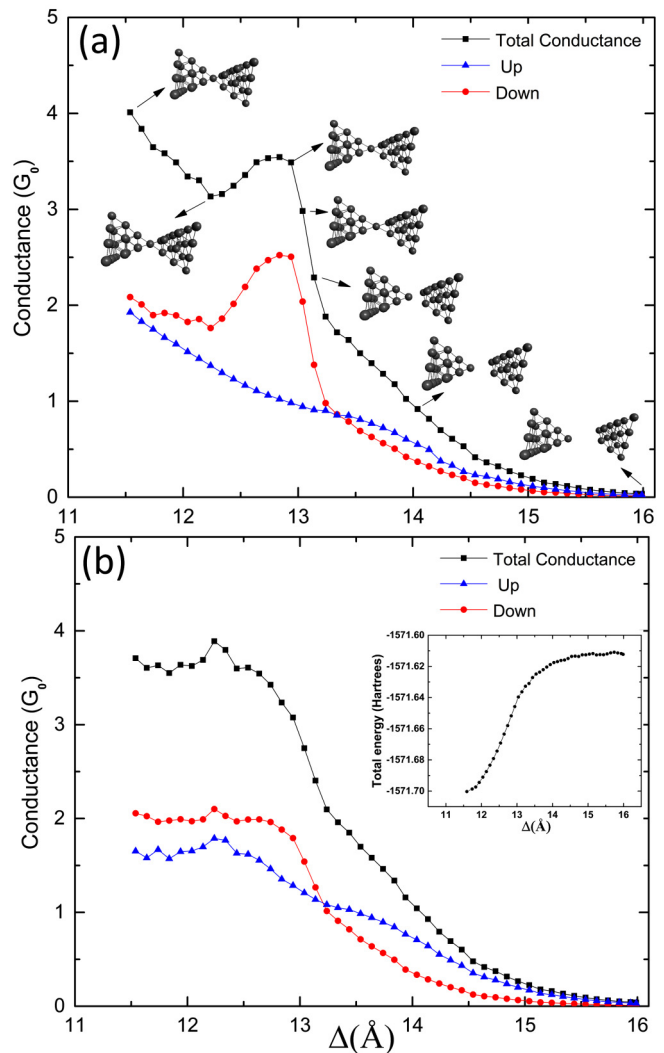


FIG. 4. Spin-resolved and total conductance at  $E_F$  as a function of electrodes distance for a monomer contact based on an fcc Ni(111) structure in (a) parallel and (b) antiparallel magnetic configuration. Intermediate structures obtained in the stretching process are also shown in the upper panel. The inset of (b) shows total energy as a function of  $\Delta$ .

We have also explored the consequences on the conductance of the formation of a domain wall in the oxidized Ni nanocontact. Now, finding the most favorable location of the domain wall requires a careful evaluation of the energy and we have found that the Ni atoms connected by the O atoms always tend to be aligned. The lowest energy domain wall has been found to preferentially form away from the O atom bridge [see inset in Fig. 6(b)] favored by the asymmetric rupture. On the one hand, the large energy cost due to the presence of three Ni-Ni exchange interactions is reduced by the breakup point itself. On the other, the presence of the second O atom in the vicinity reduces the magnetic moments of some of the participating Ni atoms. This results in a fairly large and strongly spin-filtered AP conductance [see Fig. 6(b)] despite the half-metallic behavior of the P configuration. Our realistic simulation shows that the naive assumption of perfect filtering and very large MR [11] needs to be reconsidered for more

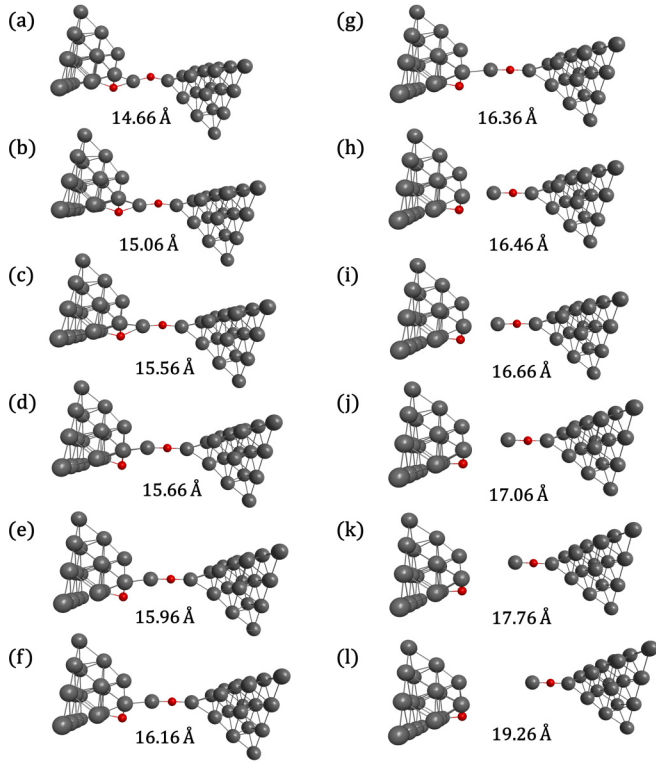


FIG. 5. Twelve relaxed structures of the oxygen contaminated dimer contact in various stages of the stretching process. The junction length  $\Delta$  during elongation is indicated below each structure.

realistic nanocontact formations as the one presented here. Nevertheless MR is still larger than in the case of pure Ni nanocontacts before the tunneling regime is reached.

#### IV. CONCLUSIONS

We have presented a systematic exploration of the influence of mechanical stretching on quantum transport in Ni nanocontacts by means of the density functional theory and nonequilibrium Green's function method. We have shown that, for both dimer and monomer structures, the more likely configurations in the final process of breaking a pure Ni contact, a plateau around  $\sim 3G_0$  can be obtained, in agreement with the existing experimental measurements [9,39]. When O atoms are added to the nanocontact, our findings predict half-metallicity (a fully spin-polarized transport) as a robust effect over the whole range in the formation process of the nanocontact, from the appearance of the last conductance plateau all the way up to the tunneling regime. An increase of the stability of the nanocontact upon the inclusion of O atoms is also obtained, as reported in experiments [39].

Previous studies [11,13] on simple nanocontact models predicted very large polarization along with huge magnetoresistance values in oxidized nanocontacts due to the presence of *ad hoc* domain walls placed near the O atoms. A closer exploration of the energy of the different possibilities for domain wall formation reveals that the position of the domain wall is more likely to take place away from the O atoms, which decreases the influence of the domain wall on transport and considerably reduces the effect. Therefore, this finding opens

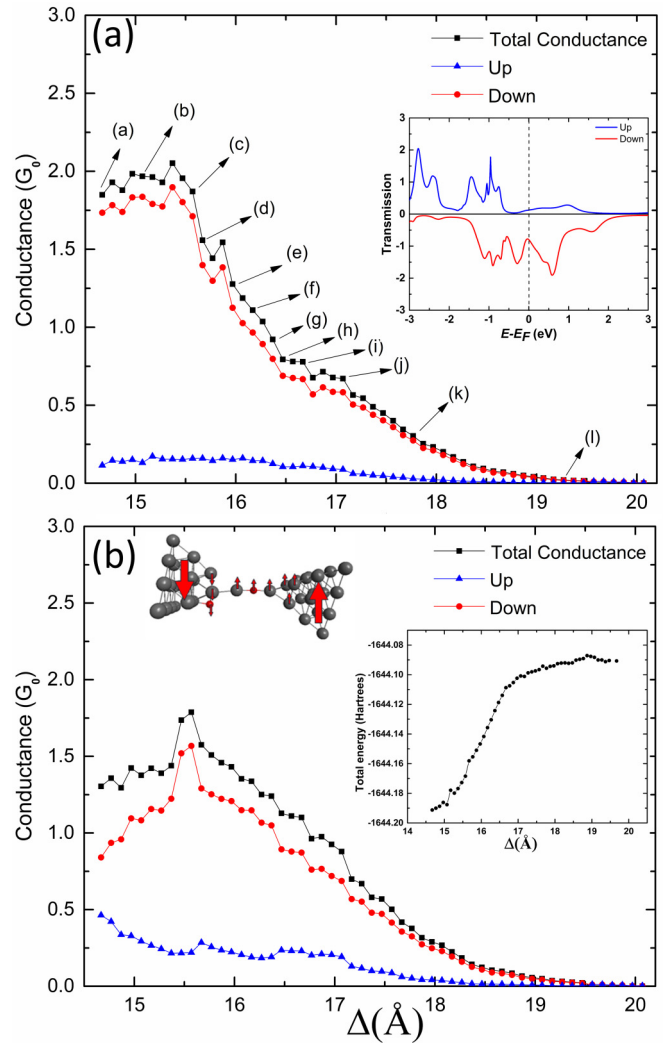


FIG. 6. Spin-resolved and total conductance at  $E_F$  as a function of electrodes displacement for O contaminated dimer contact based on an fcc Ni(111) structure in the (a) parallel and (b) antiparallel magnetic configuration. Marked black squares (a)–(l) represent the conductance values of the structures shown in Figs. 5(a)–5(l), respectively. The inset of (a) shows spin-resolved transmission as a function of energy in the parallel magnetic configuration. Total energy as a function of  $\Delta$  and the spin texture of the structure in Fig. 5(g) have been shown as insets of (b).

the way to the realization of mechanically tuned magnetic nanocontact devices for generation of more realistic spin-filtering effects and magnetoresistance ratios.

#### ACKNOWLEDGMENTS

J.J.P. acknowledges financial support from Spanish MINECO through Grant No. FIS2016-80434-P, the Fundación Ramón Areces, the María de Maeztu Program for Units of Excellence in R&D (CEX2018-000805-M), the Comunidad Autónoma de Madrid through the Nanomag COST-CM Program (No. S2018/NMT-4321), and the European Union Seventh Framework Programme under Grant Agreement No. 604391 Graphene Flagship. Z.R. acknowledges the computer resources and assistance provided by

the Centro de Computación Científica of the Universidad Autónoma de Madrid and the computer resources at MareNostrum and the technical support provided by the Barcelona Supercomputing Center (FI-2019-2-0007). A.S. and Z.R.

gratefully acknowledge computational resources provided by WestGrid, and Compute Canada. Z.R. thanks the Ministry of Science, Research and Technology of Iran for the financial support.

- 
- [1] S. Datta, in *The Oxford Handbook of Nanoscience and Technology*, Volume I: Basic Aspects, edited by A. V. Narlikar and Y. Y. Fu (Oxford University Press, Oxford, 2010)
- [2] A. Saffarzadeh, F. Demir, and G. Kirczenow, *Phys. Rev. B* **89**, 045431 (2014).
- [3] Y.-H. Kim, S. Hu, J. Lee, M. Tsutsui, and T. Kawai, *J. Am. Chem. Soc.* **139**, 8286 (2017).
- [4] C. Bruot, J. Hihath, and N. Tao, *Nat. Nanotechnol.* **7**, 35 (2012).
- [5] M. Johnson and R. H. Silsbee, *Phys. Rev. Lett.* **55**, 1790 (1985).
- [6] M. N. Baibich, J. M. Broto, A. Fert, F. Nguyen Van Dau, F. Petroff, P. Etienne, G. Creuzet, A. Friederich, and J. Chazelas, *Phys. Rev. Lett.* **61**, 2472 (1988).
- [7] G. Binasch, P. Grünberg, F. Saurenbach, and W. Zinn, *Phys. Rev. B* **39**, 4828 (1989).
- [8] J. L. Costa-Krämer, *Phys. Rev. B* **55**, R4875(R) (1997).
- [9] C. Untiedt, D. M. T. Dekker, D. Djukic, and J. M. van Ruitenbeek, *Phys. Rev. B* **69**, 081401(R) (2004).
- [10] D. Jacob, J. Fernández-Rossier, and J. J. Palacios, *Phys. Rev. B* **71**, 220403(R) (2005).
- [11] D. Jacob, J. Fernández-Rossier, and J. J. Palacios, *Phys. Rev. B* **74**, 081402(R) (2006).
- [12] J. Fernández-Rossier, D. Jacob, C. Untiedt, and J. J. Palacios, *Phys. Rev. B* **72**, 224418 (2005).
- [13] A. R. Rocha, T. Archer, and S. Sanvito, *Phys. Rev. B* **76**, 054435 (2007).
- [14] M. Häfner, J. K. Viljas, D. Frustaglia, F. Pauly, M. Dreher, P. Nielaba, and J. C. Cuevas, *Phys. Rev. B* **77**, 104409 (2008).
- [15] M. R. Calvo, J. Fernández-Rossier, J. J. Palacios, D. Jacob, D. Natelson, and C. Untiedt, *Nature* **458**, 1150 (2009).
- [16] C. Untiedt, M. J. Caturla, M. R. Calvo, J. J. Palacios, R. C. Segers, and J. M. van Ruitenbeek, *Phys. Rev. Lett.* **98**, 206801 (2007).
- [17] M. R. Calvo, M. J. Caturla, D. Jacob, C. Untiedt, and J. J. Palacios, *IEEE Trans. Nanotechnol.* **7**, 165 (2008).
- [18] R. Vardimon, M. Matt, P. Nielaba, J. C. Cuevas, and O. Tal, *Phys. Rev. B* **93**, 085439 (2016).
- [19] A. M. Bratkovsky, A. P. Sutton, and T. N. Todorov, *Phys. Rev. B* **52**, 5036 (1995).
- [20] R. Requist, P. P. Baruselli, A. Smogunov, M. Fabrizio, S. Modesti, and E. Tosatti, *Nat. Nanotechnol.* **11**, 499 (2016).
- [21] B. Olivera, C. Salgado, J. L. Lado, A. Karimi, V. Henkel, E. Scheer, J. Fernández-Rossier, J. J. Palacios, and C. Untiedt, *Phys. Rev. B* **95**, 075409 (2017).
- [22] Y.-Q. Xie, Q. Li, L. Huang, X. Ye, and S.-H. Ke, *Appl. Phys. Lett.* **101**, 192408 (2012).
- [23] I. N. Sivkov, O. O. Brovko, D. I. Bazhanov, and V. S. Stepanyuk, *Phys. Rev. B* **89**, 075436 (2014).
- [24] D. Rakhmievitch, S. Sarkar, O. Bitton, L. Kronik, and O. Tal, *Nano Lett.* **16**, 1741 (2016).
- [25] D. Li, R. Banerjee, S. Mondal, I. Maliyov, M. Romanova, Y. J. Dappe, and A. Smogunov, *Phys. Rev. B* **99**, 115403 (2019).
- [26] A. Smogunov and Y. J. Dappe, *Nano Lett.* **15**, 3552 (2015).
- [27] D. Li, Y. J. Dappe, and A. Smogunov, *Phys. Rev. B* **93**, 201403(R) (2016).
- [28] S. Li, Y.-Q. Xie, and Y. Hu, *Frontiers Phys.* **12**, 127305 (2017).
- [29] D. Djukic and J. M. van Ruitenbeek, *Nano Lett.* **6**, 789 (2006).
- [30] K. S. Thygesen and K. W. Jacobsen, *Phys. Rev. Lett.* **94**, 036807 (2005).
- [31] Y. Li, F. Demir, S. Kaneko, S. Fujii, T. Nishino, A. Saffarzadeh, G. Kirczenow, and M. Kiguchi, *Phys. Chem. Chem. Phys.* **17**, 32436 (2015).
- [32] O. Tal, M. Krieger, B. Leerink, and J. M. van Ruitenbeek, *Phys. Rev. Lett.* **100**, 196804 (2008).
- [33] A. P. F. Nascimento, M. A. San-Miguel, and E. Z. da Silva, *Phys. Rev. B* **89**, 085417 (2014).
- [34] X. Zheng, Y.-Q. Xie, X. Ye, and S.-H. Ke, *J. Appl. Phys.* **117**, 043902 (2015).
- [35] W. Thijssen, M. Strange, J. Aan de Brugh, and J. van Ruitenbeek, *New J. Phys.* **10**, 033005 (2008).
- [36] D. Li, *Phys. Rev. B* **99**, 174438 (2019).
- [37] R. H. M. Smit, C. Untiedt, A. I. Yanson, and J. M. van Ruitenbeek, *Phys. Rev. Lett.* **87**, 266102 (2001).
- [38] Y. García, J. J. Palacios, E. SanFabián, J. A. Vergés, A. J. Pérez-Jiménez, and E. Louis, *Phys. Rev. B* **69**, 041402(R) (2004).
- [39] R. Vardimon, M. Klionsky, and O. Tal, *Nano Lett.* **15**, 3894 (2015).
- [40] A. von Bieren, A. K. Patra, S. Krzyk, J. Rhensius, R. M. Reeve, L. J. Heyderman, R. Hoffmann-Vogel, and M. Kläui, *Phys. Rev. Lett.* **110**, 067203(R) (2013).
- [41] R. M. Reeve, A. Loescher, H. Kazemi, B. Dupé, M.-A. Mawass, T. Winkler, D. Schönke, J. Miao, K. Litzius, N. Sedlmayr, I. Schneider, J. Sinova, S. Eggert, and M. Kläui, *Phys. Rev. B* **99**, 214437 (2019).
- [42] J. M. Krans, C. J. Muller, I. K. Yanson, T. C. M. Govaert, R. Hesper, and J. M. van Ruitenbeek, *Phys. Rev. B* **48**, 14721 (1993).
- [43] J. M. Krans, J. M. van Ruitenbeek, and L. J. de Jongh, *Physica B* **218**, 228 (1996).
- [44] A. Halbritter, P. Makk, S. Mackowiak, S. Csonka, M. Wawrzyniak, and J. Martinek, *Phys. Rev. Lett.* **105**, 266805 (2010).
- [45] J. J. Palacios, A. J. Pérez-Jiménez, E. Louis, and J. A. Vergés, *Phys. Rev. B* **64**, 115411 (2001).
- [46] J. J. Palacios, A. J. Pérez-Jiménez, E. Louis, E. San Fabián, and J. A. Vergés, *Phys. Rev. B* **66**, 035322 (2002).
- [47] J. J. Palacios, D. Jacob, M. Soriano, W. Dednam, E. Louis, J. A. Vergés, E. SanFabián and J. A. Pérez-Jiménez, Computer code ANT.G is publicly available at <http://www.simuneatomistics.com>.
- [48] M. J. Frisch, G. W. Trucks, H. B. Schlegel, G. E. Scuseria, M. A. Robb, J. R. Cheeseman, G. Scalmani, V. Barone, B.

- Mennucci, G. A. Petersson, H. Nakatsuji, M. Caricato, X. Li, H. P. Hratchian, A. F. Izmaylov, J. Bloino, G. Zheng, J. L. Sonnenberg, M. Hada, M. Ehara *et al.*, The GAUSSIAN 09 Revision: A.02 computer code was used.
- [49] T. C. Leung, C. T. Chan, and B. N. Harmon, *Phys. Rev. B* **44**, 2923 (1991).
- [50] I. P. R. Moreira, F. Illas, and R. L. Martin, *Phys. Rev. B* **65**, 155102 (2002).
- [51] Z.-Y. Tan, X.-l. Zheng, X. Ye, Y.-q. Xie, and S.-H. Ke, *J. Appl. Phys.* **114**, 063711 (2013).
- [52] A. Burtzloff, A. Weismann, M. Brandbyge, and R. Berndt, *Phys. Rev. Lett.* **114**, 016602 (2015).